Int. J. Heat Mass Transfer. Vol. 35, No. 3, pp. 719–726, 1992
Printed in Great Britain

0017–9310/92 $5.00 + 0.00
Pergamon Press plc

Short-pulse laser heating on metals†

T. Q. QIU and C. L. TIEN
Department of Mechanical Engineering, University of California, Berkeley, CA 94720, U.S.A.

Abstract—This work analyzes microscopic radiation–metal interactions in short-pulse laser heating processes and their effects on the material thermal response. The radiation–metal interactions are treated as a coupled two-step process: (1) the absorption of photon energy by electrons and (2) the subsequent heating of the metal lattice through electron–phonon collisions. Key parameters, pulse duration to relaxation, relaxation to diffusion, and heating intensity, are introduced to classify this two-step heating regime and the conventional one-step heating regime. In the two-step heating regime, the microscopic energy transfer among photons, electrons and phonons enlarges the size of the heat-affected region and lowers the peak metal lattice temperature rise significantly. The predicted transient reflectivity changes agree with sub-picosecond laser heating experiments.

INTRODUCTION

NEW TECHNOLOGIES based on fast laser heating are developing rapidly due to increasing availability of high-power short-pulse lasers. Examples in metal processing are laser micro-machining [1], laser patterning [2], laser processing of diamond films from carbon ion implanted copper substrates [3], and laser surface hardening. In these systems, short-pulse energy deposition reduces heat-affected areas by minimizing heat diffusion and realizes ultrafast and temporally-spatially controlled heating, melting and solidification. In addition, short-pulse laser heating is becoming an important tool in studying thin film thermal properties. Since the heat diffusion penetration depth is small during a short-pulse laser heating, e.g., of the order of nanometers during a picosecond pulse, the influence of substrate on measurement is negligible [4, 5]. A better understanding of radiation–metal interactions and the associated energy transfer is critical to the performance evaluation and improvement of these technologies.

Conventional laser heating processes, which involve a relatively low energy flux and a long laser pulse, have been successfully modeled in metal processing [6] and in measuring the thin film thermal diffusivity [7]. However, the appropriateness of applying these models to short-pulse laser heating is subject to question. Human [8] and Glass *et al.* [9] applied the hyperbolic heat conduction (HHC) model in fast heating. The temperature predicted from the HHC model is significantly higher than that predicted from the conventional parabolic heat conduction model. However, the physical basis of the HHC model and its fundamental parameters (i.e., the heat wave velocity) are not clear [10]. As laser pulse duration approaches the microscopic relaxation times among different energy carriers, the mechanism of radiation absorption becomes important. This is reinforced by the observation of a thermal non-equilibrium state between electrons and the metal lattice in sub-picosecond laser heating experiments [11, 12].

The objective of the current work is to analyze the microscopic processes in radiation–metal interactions and to explore their effects on the spatial and temporal responses of the metal lattice temperature to short-pulse laser irradiation. Electrons and the metal lattice (phonons) in metals are considered as two separate systems. Electrons absorb the photon energy and then heat up the metal lattice through electron–phonon collisions.

TWO-STEP MODEL FOR RADIATION–METAL INTERACTIONS

Electromagnetic radiation with wavelength ranging from UV to near IR interacts with metals through electron excitation and electron–phonon interactions. Photons excite electrons into higher energy levels, and then the excited electrons thermalize rapidly, giving rise to a hot free electron gas. The high temperature electron gas diffuses inside the metal and then heats up the metal lattice through electron–phonon collisions. At room temperature, the collision time is about 20 femtoseconds. Due to the large difference between electron and phonon momentum, an effective energy exchange between electrons and phonons requires several tens of collisions. Therefore, the electron–phonon thermal relaxation time is of the order of picoseconds.

When the laser pulse duration is much longer than the electron–phonon thermal relaxation time, the hot electrons have enough time to establish local thermal equilibrium with the lattice. Consequently, electrons and the lattice have the same temperature T. The

† Dedicated to Professor Dr.-Ing. Dr.-Ing.e.h. Ulrich Grigull.

NOMENCLATURE

C	heat capacity [J m^{-3} K^{-1}]
C_c	heat capacity number, $C_c = C_{e0}/C_l$
D_1	first relaxation to diffusion number, $D_1 = t_c/t_{d1}$
D_2	second relaxation to diffusion number, $D_2 = t_c/t_{d2}$
f	dimensionless source term
G	electron–phonon coupling factor [W m^{-3} K^{-1}]
h	Planck constant [J s]
J	laser energy flux [J m^{-2}]
K	thermal conductivity [W m^{-1} K^{-1}]
k	Boltzmann constant [J K^{-1}]
L	film thickness [m]
l	dimensionless film thickness
m	mass [kg]
n	number density [m^{-3}]
N	pulse duration to relaxation number, $N = t_p/t_c$
Q	source term [W m^{-3}]
R	metal surface reflectivity
S	heating intensity number, $S = 0.94(1-R)J/T_0C_{e0}\delta$
T	temperature [K]
T_D	Debye temperature [K]
t	time [s]
t_c	characteristic electron–phonon thermal relaxation time , $t_c = C_{e0}/G$ [s]
t_{d1}	first diffusion time, $t_{d1} = \delta^2 C_{e0}/K$ [s]
t_{d2}	second diffusion time, $t_{d2} = L^2 C_{e0}/K$ [s]
t_p	laser pulse duration [s]
v	speed of sound [m s^{-1}]
x	spatial coordinate [m].

Greek symbols

γ	electron heat capacity constant [J m^{-3} k^{-2}]
δ	radiation penetration depth [m^{-1}]
ζ	dimensionless time
η	dimensionless spatial coordinate
θ	dimensionless temperature
σ	electrical conductivity [Ω^{-1} m^{-1}]
τ	electron mean free time between collisions [s].

Subscripts

a	atom
e	electron
l	lattice
0	reference temperature.

effects of microscopic photon–electron and electron–phonon interactions are insignificant, and the laser heating can be modeled by the conventional one-step process as

$$C(T)\frac{\partial T}{\partial t} = \nabla\cdot(K\nabla T) + Q. \tag{1}$$

In this one-step heating model, radiation heats up the material directly where it is absorbed.

When the laser-pulse duration is comparable with the electron–phonon thermal relaxation time, the electron–phonon interaction becomes an important controlling mechanism in the transfer of radiation energy to internal energy of the material. Since the electron heat capacity is small, electrons can be heated to a very high temperature with a laser of modest intensity in a very short time. Electrons and the lattice are then no longer in local thermal equilibrium and have to be considered as two separate systems. This non-equilibrium radiation heating process can be modeled phenomenologically as a two-step process: (1) the absorption of photon energy by electrons and (2) the heating of the lattice through electron–phonon coupling [13]

$$C_e(T_e)\frac{\partial T_e}{\partial t} = \nabla\cdot(K\nabla T_e) - G(T_e - T_l) + Q \tag{2a}$$

$$C_l(T_l)\frac{\partial T_l}{\partial t} = G(T_e - T_l) \tag{2b}$$

where T_e is the electron temperature and T_l is the lattice temperature. The energy transport by phonons is neglected, since heat flux is carried mainly by free electrons for metals. The electron heat capacity C_e is proportional to T_e, $C_e(T_e) = \gamma T_e$, as long as T_e is much smaller than the Fermi temperature, which is of the order of 10^4 K.

The electron–phonon coupling factor, G, is the key parameter governing the rate of the electron–phonon thermal relaxation process and can be calculated from free electron theory [14, 15]. If the lattice temperature is not much smaller than the Debye temperature T_D, the original integral expression of G [14] can be expressed approximately as

$$G = \frac{\pi^2 m_e n_e v^2}{6\tau(T_e)T_e} \tag{3}$$

where $\tau(T_e)$ is the electron mean free time between collisions at temperature T_e. If $T_l > 0.48T_D$, the error of this approximation is within 6%. For pure metals at room temperature, τ is dominated by collisions between electrons and phonons, and is inversely proportional to T_e. Therefore, G depends weakly on T_e. Within the limits of applicability of Wiedemann–Franz's law, G can be further expressed in thermal conductivity as

$$G = \frac{\pi^4(n_e v k)^2}{K}. \tag{4}$$

Table 1. Electron–phonon coupling factor G (in units of 10^{16} W m^{-3} K^{-1})

	Calculated	Measured		Calculated	Measured
Cu	14	4.8±0.7† (10‡)	V	648††	523±37†
Ag	3.1	2.8§	Nb	138††	387±36†
Au	2.6	2.8±0.5†	Ti	202¶	185±16†
Cr	45‖	42±5†	Pb	62	12.4±1.4†
W	27¶	26±3†			

† Brorson *et al.* [16].
‡ Elsayed-Ali *et al.* [17].
§ Groeneveld *et al.* [18].
‖ $n_e/n_a = 0.5$
¶ $n_e/n_a = 1.0$.
†† $n_e/n_a = 2.0$.

Table 1 presents G for several common metals. The measured values are taken from the literature [16–18] and the calculated values are from equation (4) with reported physical constants [19]. The speed of sound is evaluated from T_D and the atomic number density n_a [19].

$$v = \frac{k}{2\pi h}(6\pi^2 n_a)^{-1/3} T_D. \tag{5}$$

The number of free electrons in noble metals is taken as one per atom. For transition metals, since the exact number of free electrons contributed from the valence electrons in not clear [20], n_e is chosen by physical reasoning. The valence electrons in transition metals are divided between the s-band and the d-band. Due to the large effective mass of d-band electrons and the strong interaction between the s-band and the d-band electrons, the contribution of d-band electrons to the number of free electrons is small and only part of s-band electrons can be viewed as free electrons. Therefore, n_e is chosen here as a fraction of the valence electrons.

The calculated values of G generally agree with measured values. Metals with higher free electron number density and higher T_D have larger G values and shorter thermal relaxation times.

SHORT-PULSE LASER HEATING OF A METAL FILM

Short-pulse laser heating of a metal film is analyzed on the basis of a one-dimensional model, since the beam diameter is typically much larger than the heat diffusion penetration depth in a very short time. The temporal shape of the laser pulse is assumed to be Gaussian with an FWHM (full width at half maximum) pulse duration t_p, peaking at time zero. Because the laser pulse duration is of the order of picoseconds, heat losses from the film surfaces are negligible. By neglecting the temperature dependence of both the thermal conductivity and the lattice heat capacity, the dimensionless forms of the two-step heating model (2a) and (2b) become

$$\theta_e \frac{\partial \theta_e}{\partial \zeta} = D_1 N \frac{\partial^2 \theta_e}{\partial \eta^2} - N(\theta_e - \theta_l) + Sf(\eta, \zeta) \tag{6a}$$

$$\frac{\partial \theta_l}{\partial \zeta} = C_c N(\theta_e - \theta_l). \tag{6b}$$

Equation (6a) is non-linear because of the linear dependence of C_e on T_e. Dimensionless variables and characteristic times are defined as

$$\theta_e = T_e/T_0, \quad \theta_l = T_l/T_0, \quad \zeta = t/t_p, \quad \eta = x/\delta \tag{7a}$$

$$l = L/\delta, \quad t_{d1} = \delta^2 C_{e0}/K, \quad t_{d2} = L^2 C_{e0}/K \tag{7b}$$

where t_p is the laser-pulse duration and δ is the radiation penetration depth.

The diffusion times t_{d1} and t_{d2} are based on δ and the film thickness, L, respectively. The characteristic time for electrons and phonons to reach thermal equilibrium, t_c, can be derived from equations (6a) and (6b) by further neglecting the temperature dependence of C_e and the transport of electrons, assuming t_p to be infinitely small, and using the fact that $C_l \gg C_e$, as

$$t_c = C_e/G. \tag{8}$$

The initial time is chosen as $\zeta = -2$. The relative error of the total laser energy fluence caused by this choice is within 10^{-4}. The initial and boundary conditions are

$$\theta_e(\eta, -2) = \theta_l(\eta, -2) = 1 \tag{9a}$$

$$\left.\frac{\partial \theta_e}{\partial \eta}\right|_{\eta=0} = \left.\frac{\partial \theta_e}{\partial \eta}\right|_{\eta=1} = \left.\frac{\partial \theta_l}{\partial \eta}\right|_{\eta=0} = \left.\frac{\partial \theta_l}{\partial \eta}\right|_{\eta=1} = 0. \tag{9b}$$

The source term cannot be properly determined because of complex radiation–material interactions. As a first approximation, the problem here is simplified by neglecting the dependence of optical properties of metals on: (1) light intensity, (2) the laser pulse duration, and (3) temperature. The first assumption is applicable for modest laser intensities, e.g. 0.1–100 MW cm^{-2}, since multi-photon absorption is negligible in this intensity range [21]. The second assumption is tenable if the laser pulse duration is much larger than the electron–phonon collision time, which is about 0.02 ps at room temperature. Currently, most high-power short-pulse lasers operate in the wavelength range from 0.2 to 0.7 μm. In this range, the temperature dependence of optical prop-

Table 2. Physical constants of gold usd in calculations

Reflectivity (R)	0.93†
Radiation penetration depth (δ)	15.3 nm†
Thermal conductivity (K)	315 W m^{-1} K^{-1} [25]
Initial temperature (T_0)	300 K
Lattice heat capacity (C_l)	2.5×10^6 J m^{-3} K^{-1} [25]
Electron heat capacity (C_{e0})	2.1×10^4 J m^{-3} K^{-1} [19]
Electron–phonon coupling factor (G)	2.6×10^{16} W m^{-3} K^{-1} (Table 1)

† Typical values for visible light [25].

erties is typically small for most metals before melting. For example, the maximum temperature coefficient of reflectivity for Au, Cu, Al and Ni is of the order of 10^{-5} K^{-1} in this wavelength range [5, 22–25]. Therefore, the third assumption is acceptable. Under these assumptions, the dimensionless source term, $f(\eta,\zeta)$, can be expressed as

$$f(\eta,\zeta)=\exp(-\eta-2.77\zeta^2). \tag{10}$$

The two step-radiation heating process is governed by five parameters, the pulse-duration to relaxation number N, the first relaxation to diffusion number D_1, the second relaxation to diffusion number D_2, the heat capacity number C_c and the heating intensity number S, defined as

$$N=t_p/t_c,\quad D_1=t_c/t_{d1},\quad D_2=t_c/t_{d2} \tag{11a}$$

$$C_c=C_{e0}/C_l,\quad S=0.94(1-R)J/T_0C_{e0}\delta. \tag{11b}$$

The number N measures the relative importance of microscopic relaxation processes during laser heating. If N is much larger than one, the two-step radiation heating model reduces to the conventional one-step heating model. The numbers D_1 and D_2 characterize the effect of electron transport and the effect of the film size on the two-step heating respectively. If $D_1 \ll 1$, electrons and phonons reach thermal equilibrium before electrons can carry energy out of the radiation absorption region; therefore, the effect of electron transport on the two-step heating is small. Similarly, if $D_2 \ll 1$, the effect of the film thickness is also insignificant. The number S, the ratio of the absorbed laser energy to the energy required to raise the temperature of electrons in the radiation penetration depth to a characteristic value, reveals the relative strength of laser heating.

The transient electron and lattice temperatures are solved numerically using the Crank–Nicholson scheme. Since the radiation intensity decays exponentially within the radiation penetration depth, a non-uniform grid system is used. The electron and lattice temperatures are iterated for each time step until convergence criteria ($\Delta\theta_e < 10^{-4}$ and $\Delta\theta_l < 10^{-5}$) are satisfied. The global energy balance, based on the total increase of internal energy and the total absorbed radiation energy determined from the laser energy flux, is also checked during the computation. The material used in the simulation is gold. Its physical constants used in calculations are listed in Table 2.

RESULTS AND DISCUSSION

Short-pulse heating of a gold film

Figure 1 shows the lattice temperature profiles in a 0.5 μm gold slab during the heating of a 10 picosecond laser pulse. The temperature profiles predicted from the two-step model and the conventional one-step model are distinctly different. The absorbed radiation energy calculated from the one-step model is confined mostly within the radiation penetration depth during the laser pulse, while the two-step model predicts a much larger heat diffusion region. As a consequence, the peak lattice temperature rise from the two-step model is only half of that from the one-step model. These differences could be very important in processes in which the temperature and the size of heated area need to be precisely controlled, such as laser sputtering [26] and laser chemical processing [27]. The surface temperature also responds to the heating pulse differently. The surface temperature predicted from the one-step model begins to fall at $t = 5$ ps, which is near the end of the laser pulse. However, the temperature predicted from the two-step model is still increasing at this instant, because the microscopic photon–electron and electron–phonon interactions delay the lattice response to the heating pulse.

The electron temperature profiles are plotted in Fig. 2. The peak electron temperature rise is one order of magnitude larger than the peak lattice temperature rise (see Fig. 1), and electrons and phonons are strongly out of thermal equilibrium. These results show that there exists strong non-equilibrium heating effects even when t_p is two orders of magnitude larger than the electron mean free time between collisions.

It is also interesting to compare the two-step radi-

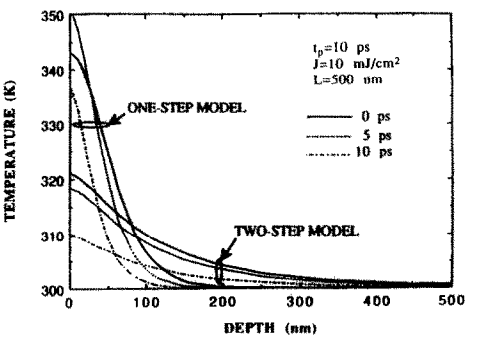

FIG. 1. Lattice temperature profiles during a 10 ps laser pulse.

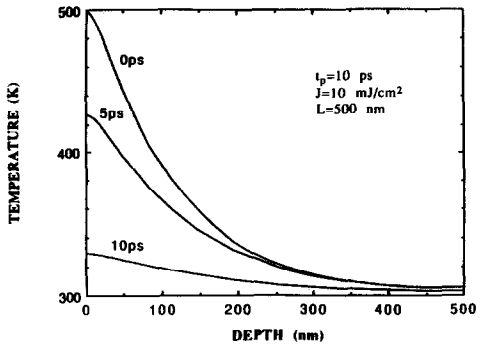

FIG. 2. Electron temperature profiles during a 10 ps laser pulse.

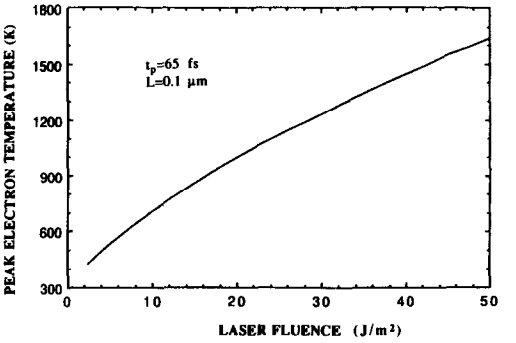

FIG. 4. Peak electron temperature as a function of laser fluence.

ation heating model and the HHC model in short-pulse laser heating. The two-step model predicts a much lower lattice temperature rise and a larger heat-affected area compared to the one-step model; on the contrary, the HHC model indicates a significantly higher temperature rise and a smaller heat-affected area [8, 9, 28]. These differences may be caused by the fact that the HHC model totally neglects the microscopic processes of energy transfer among different energy carriers.

Figure 3 presents the temperature profiles in a 1 μm gold film during the heating of a one nanosecond laser pulse. The lattice and electron temperatures predicted from the two-step model converge to the temperatures from the one-step model, indicating that the effects of the microscopic radiation–metal interactions become less important for laser pulse durations of the order of nanoseconds.

Comparison with experiments

Different laser heating models can be tested by short-pulse laser heating experiments [29, 30]. In these experiments, a pump laser beam heats gold films, and a probe laser beam measures the transient reflectivity change ΔR. The probe laser photons excite the electrons in the completely filled valance d-band to the half-filled conduction band near the Fermi level. The electron and lattice temperatures affect the reflectivity by modifying (1) the electron number density in the final state of the excitation and (2) the band structure. Theoretically, optical properties of gold can be calculated from the band structure and the electron number density distribution [31, 32]; however, due to the uncertainties in the band parameters, the calculated optical properties do not agree with experimental data quantitatively [32, 33]. Therefore, in this study, the relation between ΔR and temperature changes is established by physical reasoning and experimental observation.

At the early stage of a short-pulse laser heating, due to the delay of the lattice temperature rise compared with the electron temperature rise ΔT_e, the lattice temperature rise is small; therefore, ΔR is mainly caused by ΔT_e. The maximum reflectivity change $(\Delta R)_{max}$ varies linearly with laser fluence [29, 30]; in addition, the peak electron temperature rise $(\Delta T_e)_{max}$, predicted from the two-step radiation heating model, varies almost linearly with laser fluence (Fig. 4). Therefore, ΔR can be assumed to be proportional to ΔT_e, and

$$\Delta R/(\Delta R)_{max} = \Delta T_e/(\Delta T_e)_{max}. \quad (12)$$

Figures 5 and 6 present the comparison of predicted $\Delta R/(\Delta R)_{max}$ from equation (12) with that from sub-picosecond laser heating experiments [29]. $\Delta T_e/(\Delta T_e)_{max}$ is evaluated from the one-step and the two-step radiation heating models respectively. The results from the two-step model agree with experiments, but the one-step model fails to predict the fast energy

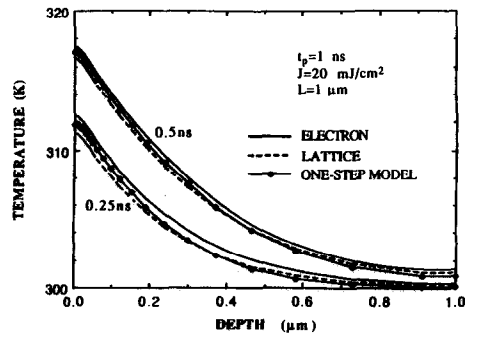

FIG. 3. Temperature profiles during a 1 ns laser pulse.

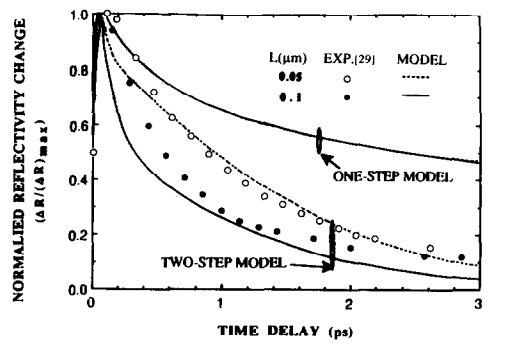

FIG. 5. Transient reflectivity changes at the front surface (t_p = 96 fs, J = 1 mJ cm^{-2}).

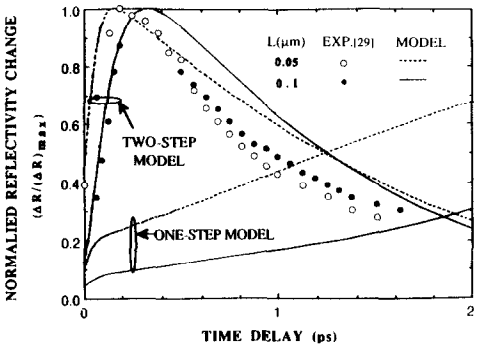

FIG. 6. Transient reflectivity changes at the rear surface ($t_p = 96$ fs, $J = 1$ mJ cm^{-2}).

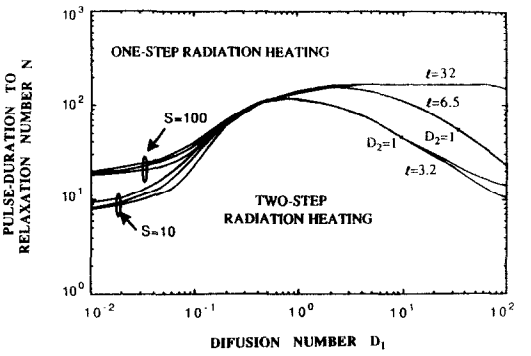

FIG. 7. Regime map for one-step and two-step radiation heating.

transport process and the rapid electron–phonon relaxation process at the rear surface of the film.

At the front surface, both the electron transport process and the electron–phonon relaxation process remove the energy from the electrons within the radiation penetration depth, which in turn decreases the surface electron temperature. Increasing the film thickness enhances the transport process; thus, the drop of the surface electron temperature becomes more rapid. At the rear surface, T_e rises with the arrival of the heat wave transported by electrons, and then decreases due to the electron–phonon relaxation. The time for ΔT_e to reach maximum reduces with decreasing film thickness.

Regime map for one-step and two-step radiation heating

The short-pulse laser heating process is characterized by six parameters: N, D_1, D_2, C_e, l, and S. The typical ranges of these parameters are 0.01–100 for D_1, 0–5 for D_2, 1–1000 for l, and 1–1000 for S. Since the heat capacity number C_e varies only slightly for different materials, C_e is taken as 8.5×10^{-3} in this study.

In long-pulse laser heating, the one-step model is valid; in short-pulse laser heating, the two-step radiation heating model should be applied. A critical number N_{cr} is defined to separate these two regimes quantitatively. It is defined as the number N at which the prediction of surface temperature from the one-step radiation model causes a 20% error compared with the two-step radiation heating model.

Figure 7 shows the regime map for one-step and two-step radiation heating based on these parameters. N_{cr} is affected by the transport of electrons, the heating intensity, and the size of the film. As D_1 approaches zero, the effect of transport becomes small; thus N_{cr} approaches one. As D_1 increases, the transport process, which competes with the electron–phonon relaxation process, becomes important, as a result, N_{cr} increases.

The number D_2 is related to D_1 by $D_2 = D_1 \cdot l^2$, and the position of $D_2 = 1$ is marked on the curves. When D_2 is much smaller than one, the size effect on N_{cr} is small since electrons cannot carry energy far enough to feel the existence of the other side of the film during the electron–phonon relaxation period. In the regime $D_1 > 1$ and $D_2 < 1$, N_{cr} is nearly constant. The size effect on N_{cr} begins near the point $D_2 = 1$. With the further increase of D_2, hot electrons can reach the rear surface of the film at the very beginning of the electron–phonon relaxation process; thus, the transport effects on N_{cr} are eliminated, and N_{cr} decreases.

When the transport effect is small ($D_1 < 0.1$), N_{cr} increases with the number S due to the non-linear dependence of T_e on S. When the transport effect is large ($D_1 > 1$), the effects of S on N_{cr} become less important because the electron transport process does not depend on the heating intensity. Since the number l only affects the transport process, it can be expected that increasing l enhances the effects of the two-step radiation heating in the region $D_1 > 1$ and has negligible effects in the region $D_1 < 0.1$.

Given the material properties and laser pulse duration, this regime map suggests the appropriate radiation heating model. Similarly, a laser pulse duration can be predicted to achieve or avoid non-equilibrium heating.

CONCLUSIONS

The effects of microscopic radiation–metal interactions on fast laser heating have been studied by using a two-step radiation heating model. In a fast heating regime (pulse duration of the order of picoseconds or shorter), the microscopic energy transfer among photons, electrons and phonons becomes very important. It enlarges the heat-affected region and lowers the peak temperature rise of the metal lattice significantly. The conventional one-step radiation heating model overpredicts the peak surface temperature and underpredicts the heat-affected region. In a slow heating regime (pulse duration of the order of nanoseconds), the two-step radiation heating model reduces to the conventional radiation heating model. The transient reflectivity changes predicted from the two-step model agree with sub-picosecond laser heating experiments. Key parameters, pulse duration to relaxation, relaxation to diffusion, and laser

heating intensity, are introduced to characterize short-pulse laser heating processes. A general regime map, based on these numbers, is constructed to demonstrate the validity of the one-step and two-step radiation heating models.

Acknowledgements—The authors gratefully acknowledge the financial support for this research from the U.S. National Science Foundation, the U.S. Department of Energy, and the K.C. Wong Education Foundation.

REFERENCES

1. J. A. Knapp, P. Børgesen and R. A. Zuhr (Editors), Beam–Solid Interactions: Physical Phenomena. *Mater. Res. Soc. Symp. Proc.*, Vol. 157. Materials Research Society, Pittsburgh (1990).
2. D. J. Elliott and B. P. Piwczyk, Single and multiple pulse ablation of polymeric and high density materials with excimer laser radiation at 193 nm and 248 nm, *Mater. Res. Soc. Symp. Proc.*, Vol. 129, pp. 627–636. Materials Research Society, Pittsburgh (1989).
3. J. Narayan, V. P. Godbole and G. W. White, Laser method for synthesis and processing of continuous diamond films on nondiamond substrates, *Science* **52,** 416–418 (1991).
4. G. L. Eesley, Picosecond dynamics of thermal and acoustic transport in metal films, *Int. J. Thermophys.* **11,** 811–817 (1990).
5. A. Miklos and A. Lorincz, Transient thermoreflectance of thin metal films in the picosecond regime, *J. Appl. Phys.* **63,** 2391–2395 (1988).
6. W. W. Duley, *Laser Processing and Analysis of Materials.* Plenum Press, New York (1983).
7. I. Hatta, Thermal diffusitivity measurements of thin films and multilayered composites, *Int. J. Thermophys.* **11,** 293–302 (1990).
8. M. Human, Non-Fourier heat transfer in laser heated metal surfaces, *Heat Transfer: Korea-U.S.A. Seminar* (Edited by J. H. Kim *et al.*), pp. 521–533 (1986).
9. D. E. Glass, M. N. Ozisik and W. S. Kim, Hyperbolic Stefan problem with applied surface heat flux and temperature-dependent thermal conductivity, *Numer. Heat Transfer* **A18,** 503–516 (1990).
10. D. D. Joseph and L. Preziosi, Heat waves, *Rev. Mod. Phys.* **61,** 41–73 (1989).
11. G. L. Eesley, Observation of non-equilibrium electron heating in copper, *Phys. Rev. Lett.* **51,** 2140–2143 (1983).
12. J. G. Fujimoto, J. M. Liu and E. P. Ippen, Femtosecond laser interaction with metallic tungsten and nonequilibrium electron and lattice temperatures, *Phys. Rev. Lett.* **53,** 1837–1840 (1984).
13. S. I. Anisimov, B. L. Kapeliovich and T. L. Perel'man, Electron emission from metal surfaces exposed to ultrashort laser pulses, *Sov. Phys. JETP* **39,** 375–377 (1974).
14. M. I. Kaganov, I. M. Lifshitz and L. V. Tanatarov, Relaxation between electrons and crystalline lattice, *Sov. Phys. JETP* **4,** 173–178 (1957).
15. P. B. Allen, Theory of thermal relaxation of electrons in metals, *Phys. Rev. Lett.* **59,** 1460–1463 (1987).
16. S. D. Brorson, A. Kazeroonian, J. S. Moodera, D. W. Face, T. K. Cheng, E. P. Ippen, M. S. Dresselhaus and G. Dresselhaus, Femtosecond room temperature measurement of the electron–phonon coupling constant λ in metallic superconductors, *Phys. Rev. Lett.* **64,** 2172–2175 (1990).
17. H. E. Elsayed-Ali, T. B. Norris, M. A. Pessot and G. A. Mourou, Time-resolved observation of electron–phonon relaxation in copper, *Phys. Rev. Lett.* **58,** 1212–1215 (1987).
18. R. H. M. Groeneveld, R. Sprik, M. Wittebrood and A. Lagendijk, Ultrafast relaxation of electrons probed by surface plasmons at a thin silver film. In *Ultrafast Phenomena VII* (Edited by C. B. Harris *et al.*), pp. 368–370. Springer, Berlin (1990).
19. C. Kittell, *Introduction to Solid State Physics*, 6th Edn. Wiley, New York (1986).
20. A. Wilson, *The Theory of Metals.* The University Press, Cambridge (1936).
21. M. M. Murnane and R. W. Falcone, Short pulse laser interaction with solid, *SPIE*, Vol. 913, *High Intensity Laser–Matter Interactions*, pp. 5–8 (1988).
22. W. J. Scouler, Temperature-modulated reflectance of gold from 2 to 10 eV, *Phys. Rev. Lett.* **18,** 445–448 (1967).
23. R. Rosei and D. W. Lynch, Thermomodulation spectra of Al, Au, and Cu, *Phys. Rev.* **B5,** 3883–3894 (1972).
24. J. Hanus, J. Feinleib and W. J. Scouler, Low-energy interband transitions and band structure in nickel, *Phys. Rev. Lett.* **19,** 16–20 (1967).
25. *American Institute of Physics Handbook*, 3rd Edn. McGraw-Hill, New York (1972).
26. R. Kelly and J. E. Rothenberg, Laser sputtering, *Nucl. Instrum. Meth.* **B7/8,** 755–763 (1985).
27. D. Bauerle, Chemical processing with lasers, *Appl. Phys.* **B46,** 261–270 (1988).
28. C. Bai and A. S. Lavine, Hyperbolic heat conduction in a super-conducting film, *ASME/JSME Thermal Engineering Proc.*, Vol. 4, pp. 87–92. ASME, New York (1991).
29. S. D. Brorson, J. G. Fujimoto and E. P. Ippen, Femtosecond electron heat-transport dynamics in thin gold film, *Phys. Rev. Lett.* **59,** 1962–1965 (1987).
30. H. E. Elsayed-Ali, Femtosecond thermoreflectivity and thermotransmissivity of polycrystalline and single-crystalline gold films, *Phys. Rev.* **B43,** 4488–4491 (1991).
31. M. Cardona, *Modulation Spectroscopy.* Academic Press, New York (1969).
32. M. Guerrisi and R. Rosei, Splitting of the interband absorption edge in Au, *Phys. Rev.* **B12,** 557–563 (1975).
33. B. R. Cooper and H. Ehrenreich, Optical properties of noble metals. II, *Phys. Rev.* **A138,** 494–507 (1965).

CHAUFFAGE DES METAUX PAR LASER A BREVE PULSATION

Résumé—On analyse les interactions microscopiques rayonnement–métal pendant le chauffage par laser à brève pulsation et leurs effets sur la réponse thermique du métal. Ces interactions sont traitées comme un mécanisme couplé à deux étapes: (1) l'absorption de l'énergie des photons par les électrons et (2) le chauffage du réseau du métal par les collisions électron–phonon. Les paramètres actifs, la durée de la pulsation et la relaxation, de la relaxation à la diffusion, l'intensité du chauffage, sont introduits pour traiter ce régime de chauffage à deux étapes et le régime conventionnel de chauffage à une seule étape. Dans le régime de chauffage à deux étapes, le transfert microscopique d'énergie parmi les photons, les électrons et les phonons augmente la dimension de la région affectée par le chauffage et diminue sensiblement le pic de température du métal. Les changements prédits de réflectivité variable s'accordent avec les expériences de chauffage laser sub-picroseconde.

ERWÄRMUNG VON METALLEN MITTELS KURZER LASERPULSE

Zusammenfassung—In der vorliegenden Arbeit wird die mikroskopische Wechselwirkung zwischen Strahlung und Metallen während einer Erwärmung mittels kurzer Laserpulse und deren Einfluß auf das thermische Verhalten des Materials untersucht. Die Wechselwirkung zwischen Strahlung und Metall wird als gekoppelter zweistufiger Prozeß behandelt: (1) Absorption von Photonenergie durch Elektronen und (2) die nachfolgende Aufheizung des Metallgitters durch Kollisionen zwischen Elektronen und Phononen. Schlüsselparameter, wie das Verhältnis der Pulsdauer zur Relaxation, der Relaxation zur Diffusion und der Intensität der Erwärmung, werden zur Klassifizierung dieses zweistufigen Erwärmungsbereichs und des herkömmlichen einstufigen Erwärmungsbereichs eingeführt. Im zweistufigen Bereich vergrößert die mikroskopische Energieübertragung zwischen Photonen, Elektronen und Phononen die Größe des wärmebeaufschlagten Bereichs, während die Temperaturspitze im Metallgitter spürbar kleiner wird. Die berechneten transienten Veränderungen des Reflexionsvermögens stimmen gut mit Laserexperimenten unterhalb des Picosekundenbereichs überein.

КОРОТКОИМПУЛЬСНЫЙ ЛАЗЕРНЫЙ НАГРЕВ МЕТАЛЛОВ

Аннотация—Анализируются микроскопические взаимодействия между излучением и металлом в процессах короткоимпульсного лазерного нагрева и их влияние на тепловые характеристики материала. Исследуемые взаимодействия рассматриваются как взаимосвязанный процесс, состоящий из двух этапов: 1) поглощение энергии фотонов электронами и 2) последующий нагрев металлической решетки при соударениях электронов и фононов. Для классификации двухступенчатого режима нагрева и режима обычного одноступенчатого нагрева вводятся такие параметры как отношение длительности импульса к времени релаксации, времени релаксации к характерному времени диффузии и интенсивность нагрева. При двухступенчатом режиме нагрева микроскопический перенос энергии между фотонами, электронами и фононами приводит к существенному увеличению размера нагреваемого участка и снижению максимальной температуры кристаллической решетки металла. Теоретические расчеты изменений нестационарного коэффициента отражения согласуются с экспериментальными данными для субпикосекундных лазеров.